Biomass Burning Aerosol Absorption Measurements with MODIS Using the Critical Reflectance Method

Zhu, L., J. V. Martins, L. A. Remer

Li Zhu

University of Maryland, Baltimore County, Department of Physics and Joint Center for Earth Systems Technology, 1000 Hilltop Circle, Baltimore, MD, 21250

410-455-1986

zhuli1@umbc.edu

Vanderlei J. Martins

University of Maryland, Baltimore County, Department of Physics and Joint Center for Earth Systems Technology, 1000 Hilltop Circle, Baltimore, MD, 21250

410-455-2764

martins@umbc.edu

Lorraine A. Remer

code 613.2, NASA Goddard Space Flight Center, Greenbelt MD 20771 USA

301-614-6194

Lorraine.A.Remer@nasa.gov

Abstract

This research uses the critical reflectance technique, a space-based remote sensing method, to measure the spatial distribution of aerosol absorption properties over land. Choosing two regions dominated by biomass burning aerosols, a series of sensitivity studies were undertaken to analyze the potential limitations of this method for the type of aerosol to be encounterd in the selected study areas, and to show that the retrieved results are relatively insensitive to uncertainties in the assumptions used in the retrieval of smoke aerosol. The critical reflectance technique is then applied to Moderate Resolution Imaging Spectrometer (MODIS) data to retrieve the spectral aerosol single scattering albedo (SSA) in South African and South American biomass burning events. The retrieved results were validated with collocated Aerosol Robotic Network (AERONET) retrievals. One standard deviation of mean MODIS retrievals match AERONET products to within ±0.03, the magnitude of the AERONET uncertainty. The overlap of the two retrievals increases to 88%, allowing for measurement variance in the MODIS retrievals as well. The ensemble average of MODIS-derived SSA for the Amazon forest station is 0.92 at 670 nm, and 0.84-0.89 for the southern African savanna stations. The critical reflectance technique allows evaluation of the spatial variability of SSA, and shows that SSA in South America exhibits higher spatial variation than in South Africa. The accuracy of the retrieved aerosol SSA from MODIS data indicates that this product can help to better understand how aerosols affect the regional and global climate.

I. Introduction

Atmospheric aerosols absorb solar radiation, warm the atmosphere (Penner et al., 1992), and cool the Earth surface (Ramanathan et al., 2001). Therefore, they disturb the atmospheric temperature profile (Ackerman et al., 2000; Ramanathan et al., 2007; Davidi et al., 2009), and affect cloud properties (Koren et al., 2004; Koren et al., 2008; Feingold et al., 2005) and precipitation (Ramanathan et al., 2001; Ramanathan et al., 2005; Menon et al., 2002). These effects are particularly important over areas with high aerosol concentration (Sato et al, 2003; Wang et al., 2004), such as the southern Africa region (Ichoku et al., 2003), the Amazon region (Procopio et al., 2004), the Asian region (Ramana & Ramanathan, 2006), and Yellow Sea, Arabian Sea, and Saharan Coast region (Zhu et al., 2007). A quantitative understanding of the role of absorbing aerosols in climate change is also required to formulate reliable policy recommendations (Hansen et al., 2000).

Aerosol absorption is typically expressed in terms of aerosol single scattering albedo ($SSA = \frac{aerosol\ scattering\ coefficient}{aerosol\ scattering\ coefficient + aerosol\ absorption\ coefficient}$). The importance of aerosol SSA to climate modification was first studied back in the 1970s (Atwater, 1970; Mitchell JR, 1971). However, even though SSA is the biggest contributor to the total uncertainty in aerosol direct radiative forcing (McComiskey et al., 2008), accurate aerosol SSA retrieval remains challenging still today (Heintzenberg et al., 1997; Moosmuller et al., 2009). Many approaches have been developed to study aerosol absorption properties, including microphysical simulations (Ackerman & Toon, 1981; Martins, et al., 1998), data analysis from AERONET (Dubovik et al., 2002), and in situ measurements (Clarke, et al., 1987; Reid, et al., 1998; Bond et al., 1999; Martins, et al., 2009), and ground based remote sensing techniques (Dubovik et al., 1998).

Space based remote sensing techniques to measure aerosol absorption have also been increasingly developed. More specifically, TOMS and combination of multi sensors on different satellites have been used to study aerosol absorption. However, the retrieval of SSA from TOMS is limited in the UV range (320-440nm), and the result is sensitive to the assumed aerosol layer height (Herman, et al., 1997; Torres, et al., 1998). Moreover, the combination of satellite sensors, such as TOMS and ERBE (Hus, et al., 2000), TOMS and MODIS (Hu, et al., 2007), OMI and MODIS (Satheesh, et al., 2009), TOMS, MODIS and MISR (Hu, et al., 2009), and A-train satellite sensors (MODIS, OMI, and CALIPSO) (Jeong & Hsu, 2008), have been used to retrieve SSA. Nevertheless, these retrievals are still limited to the UV range, and the error sources introduced by using multi platforms with different resolutions, slightly different observation times, and different calibrations have not yet been well studied.

Recently, some other space based techniques have been proposed to study aerosol absorption as well. Measuring aerosol SSA over ocean from space, by using ocean sun glint as a bright background against aerosol absorption, was proposed by Kaufman, et al., in 2002. MISR also has the ability to distinguish weakly absorbing (having 1%-4% of hematite, SSA in the range of 0.98-0.99) and strongly absorbing (having 10% hematite, red channel SSA of about 0.94) dust components (Kalashnikova, et al., 2005; Kalashnikova, et al., 2006). Moreover, based on the fact of differing sensitivities of polarized and unpolarized reflectance to aerosol absorption, Glory will be used to retrieve SSA from polarimetric measurements in a single pixel (Mishchenko, et al., 2007, Table 2). Even with these efforts, however, aerosol absorption measurement with satellite remote sensing still remains challenging and more studies are needed.

Compared with the techniques discussed above, the “critical reflectance” method is also a promising space based remote sensing technique to retrieve SSA (Fraser & Kaufman, 1985).

According to the Fraser and Kaufman (1985) radiative transfer simulations, there exists a specific surface reflectance for which increased aerosol loading (being represented here by aerosol optical depth or AOD) does not change the reflectance at the TOA (top of the atmosphere). This unchanging reflectance at the TOA is defined as the critical reflectance, which has a one-to-one relationship to aerosol SSA (Fraser & Kaufman, 1985). This technique has been utilized with several space based remote sensing instruments to retrieve aerosol SSA: (1) using Landsat Multi-Spectral Sensor Imagery as well as aircraft radiance data to retrieve aerosol SSA over the DC area (Kaufman, 1987); (2) using AVHRR images in visible and near-IR bands to retrieve the SSA of forest smoke (Kaufman, et al., 1990); (3) using Landsat TM images to retrieve dust SSA, where the result agreed well with AERONET SSA (Kaufman, et al., 2001).

This research applies the critical reflectance technique to MODIS data to retrieve aerosol SSA. The first MODIS sensor aboard NASA's Terra satellite was launched in 1999 and the second one on the Aqua satellite launched in 2002. Each MODIS sensor provides a global data set every 1-2 days with a 16-day repeat cycle. The sensors collect the Earth images at 36 spectral bands in the wavelength range from 0.4 μm to 14.4 μm with a swath width of 2330 km (cross track) and continuous along-track coverage. Specifically, the seven aerosol bands are: 0.62-0.67, 0.84-0.87, 0.46-0.48, 0.55-0.57, 1.2-1.3, 1.63-1.65, and 2.11-2.16 μm, nominally 0.67, 0.86, 0.47, 0.55, 1.24, 1.64, and 2.12 μm respectively. This research discusses how to calculate the critical reflectance from MODIS data and the sensitivity of potential factors affecting the retrieval, such as detector zenith angle (DZA) and AOD difference between the polluted day and the clean days. We also present validation results with collocated AERONET measurements as well as regional SSA maps.

II. Calculating Critical Reflectance from MODIS Data

In this section, we use two days of MODIS images 16 days apart at the AERONET Mongu site (latitude= -15.25°, longitude= 23.15°) with low AOD (0.36 at 0.67 μm) day 266 and high AOD (0.7 at 0.67 μm) day 250 in year 2000 to describe how to calculate the critical reflectance parameter. The 16 days apart are used to assume the same angular geometry. In the rest of this study, we will refer to the low AOD day as the "clean day" and the high AOD day as the "polluted day". Figure 1 shows the RGB images of the southern African region on the clean day (the image on the left) and the polluted day (the image on the right). Next, a 60 × 60 km area (latitude= [-15.545 to -14.95]; longitude= [22.85 to 23.45]; blue color box in the image on the left and the purple color box in the image on the right) centered at Mongu is selected for detailed illustration.

Prior to the calculation of the critical reflectance, the cloud mask algorithm by Martins, et al. (2002) is applied to MODIS level 1B calibrated reflectance data (0.5 km resolution). After being projected on the grid of 100 pixels per degree (approximately 1km resolution), the results on both days in the 60 × 60 km range are mapped in Fig. 2.

Next, the 3600 (60 × 60) pixels from both images in Fig. 2 are evenly divided into a 3 × 3 matrix to produce nine cells with equal numbers of 400 (20 × 20) pixels each. Then, using a scatter plot such as shown in Fig. 3 (showing the data from the first cell), we compare the reflectance from pixels in every cell on day 266 to each corresponding pixel on day 250. These data points are then fitted with a robust fit technique (the red color line in Fig. 3; DuMouchel & O'Brien, 1989), which minimizes the effect of potential outlier points. The corresponding

reflectance at the TOA that represents the crossing point between the fitted red line and the y=x black line is by definition the critical reflectance. The intercept of the fitted red color line on the y-axis is defined as the effective path radiance. Our radiative transfer simulations showed that the effective path radiance is approximately 10 times the AOD difference between the clean day and the polluted day. This result will be used later in the section describing the aerosol SSA retrieval.

III. Sensitivity Studies

Aerosol SSA can be retrieved from the measured critical reflectance by inputting aerosol models (aerosol size distribution and the real part of aerosol refractive index) on a Mie code (Wiscombe, 1980) and on a radiative transfer model (Santa Barbara DISORT Atmospheric Radiative Transfer - SBDART by Ricchiazzi, et al., 1998). To better understand this application and assess the quality of the aerosol SSA retrieval results, we developed a series of sensitivity tests and validated the results with collocated AERONET measurements. In the following sections, we show these tests and validation outcomes, discuss factors affecting the retrieval results, and display SSA maps.

Aerosol SSA can be retrieved through its unique correlation with the measured critical reflectance. This technique has the distinct advantages of possible global coverage over land, daily measurements, and the no need to know the Earth surface reflectance. It also carries the following potential limitations: (a) it requires reasonable knowledge of the involved aerosol models, (b) the critical reflectance should be AOD independent, (c) background aerosols on the clean day and aerosols on the polluted day should have the similar SSA, (d) the Earth surface must exhibit Lambertian reflectance, and (e) there needs to be a large enough AOD difference

between these two days. There are other limitations as well, such as the studied area should have enough surface reflectance variability, aerosols should be homogeneously distributed within the studied cell range, and the surface reflectance should be the same on the clean day and the polluted day. In order to understand the importance of these limitations, a series of sensitivity studies have been completed as shown in the following sub sections.

In addition, to study these sensitivities and validate aerosol SSA retrieved from MODIS, we have to use other available column aerosol SSA measurements. Furthermore, high accuracy of aerosol SSA - e.g. SSA uncertainty of 0.01 - is required to make accurate climatic predications. However, the availability of aerosol SSA measurements qualifying these two conditions is significantly limited. The Glory mission (to be launched in November 2010) by NASA might improve this situation in the future. At present, we use AERONET measurements, in which aerosol SSA uncertainty is 0.03 when AOD (at 440 nm) is greater than 0.4 (Dubovik et al., 2004), for our validation. To be consistent, we compare the uncertainty caused by each corresponding limitation also with 0.03, even though our goal is to measure aerosol SSA with much smaller uncertainty. If the difference is significantly smaller than 0.03, we regard that the limitation has little effect on the retrieved aerosol SSA and the uncertainty is acceptable; in contrast, if the difference is greater than 0.03, it indicates that the limitation significantly affects the aerosol SSA retrieval and needs to be considered in the retrieval algorithm.

(a) Aerosol Models

Aerosol models including aerosol size distribution and the real part of aerosol refractive index from the research by Dubovik et al (2002) are used here as a first guess in our SSA retrieval. These aerosol models are generated from AERONET data before 2000; however, MODIS

provides data after 2000. To see whether the models can represent the data from the years after 2000, the real part of aerosol refractive index is studied, and the result shows that the mean real part of the refractive index for biomass burning aerosols over Mongu is 1.51, which agrees well with the value of 1.51 from Dubovik et al's model (Dubovik, et al., 2002, table 1). Similar comparisons over other AERONET sites also show good agreements between the data before and after 2000. Therefore, Dubovik et al's aerosol models are used in our research to represent the aerosol properties.

In addition, the data analysis shows that the ratio of its standard deviation of the real refractive index over its mean value is approximately 2.3% over Mongu. The sensitivity study in Fig. 4 indicates that the 2.3% variation of the mean for a mean value of 1.495 (the real refractive index from AERONET retrieval over Mongu on day 250 in year 2000) leads to an aerosol SSA uncertainty of 0.01, 0.017, and 0.021 (with the imaginary refractive index as 0.012, 0.024, and 0.036 respectively, where 0.024 is the AERONET retrieved imaginary refractive index). This is an acceptable uncertainty compared to the AERONET 0.03 error. This analysis indicates that the sensitivity to real refractive index is relatively small and a relatively coarse first guess is acceptable.

(b) Dependence of Critical Reflectance on AOD

The definition of critical reflectance assumes it to be AOD independent (Fraser & Kaufman, 1985, Figure 2). Nevertheless, a closer look at the crossing point shows that the simulated lines cross each other in the neighborhood of one point, instead of exactly at that point (Kaufman, 1987), which implies that critical reflectance is weakly dependent on AOD. A sensitivity study to determine the importance of this effect was performed. According to Fig. 5, when AOD on the

polluted day increases from 0.5 to 1.0 and AOD on the clean day remains as 0.1, the variation of the critical reflectance is 0.01. This extreme case with the uncertainty of AOD between 0.5 to 1.0 leads to an SSA uncertainty of ±0.0125 (at SSA=0.8) and ±0.005 (at SSA=0.95), as in Fig.6., which are both significantly smaller than the 0.03 uncertainty from AERONET. In reality, we will have a much better handle on the AOD uncertainties and will significantly reduce these error bars.

(c) Varying Aerosol SSA on the Clean Day and on the Polluted Day

The basic critical reflectance technique also assumes that the background aerosols in both clean days and polluted days have the same SSA. However, this condition might not be satisfied. To study how aerosol SSA variation affects the retrieval results, we assume that on the polluted day aerosol SSA (at 0.67 μm) is 0.898 and AOD is 0.7, on the clean day AOD is 0.2 and SSA (on clean day) varies from 0.986 to 0.824 as in column 2 of Table. 1. The results of a similar analysis of SSA are also shown in Table 1: on the polluted day SSA is 0.972 and varies from 0.910 to 0.993 on the clean day. The real part refractive index is kept at 1.51 for both days. The results in column 5 of Table 1 show that the difference between the retrieved SSA and the SSA on the polluted day varies between -0.026 to 0.019 (when SSA on the polluted day is 0.898) and -0.006 to 0.018 (when SSA on the polluted day is 0.972). Considering these differences are still smaller than the AERONET aerosol SSA uncertainty 0.03 even under extreme cases, we regard that varying the aerosol SSA between the clean day and the polluted day affects retrieved aerosol SSA with acceptable uncertainty.

(d) DZA

The data analysis shows that detector zenith angle (DZA) affects retrieval results when it is bigger than 40 degrees. This issue can be demonstrated through the results of a group of cases over Senanga in 2000. According to Fig. 7, when DZA is greater than 40 degrees, the deviation of MODIS SSA from AERONET SSA increases as DZA increases. In addition, in order to keep the deviation below 0.03, DZA needs to be smaller than 40 degrees. This result is likely due to the fact that our retrieval applies the simplified assumption of Lambertian Earth surface reflectance, instead of the reflectance with angular distribution usually modeled by the Bi-directional Reflectance Distribution Function (BRDF) (Maignan, et al., 2004). This issue will be addressed in more detail in our future research with the incorporation of the Earth surface BRDF in radiative transfer simulations. At this point, we will only select cases with DZA< 40 degrees as a quality assurance procedure. The similar analysis of SSA with scattering angle and SSA with solar zenith angle does not show SSA dependence on these two geometries as its dependence on DZA.

(e) AOD Difference between the Clean day and the Polluted Day

Besides DZA, AOD difference (between the clean day and the polluted day) affects the signal to noise ratio and hence the accuracy of the SSA retrieval. A group of cases over Mongu in 2000 is used to study this issue. As shown in Fig.8, in order to keep the deviation of MODIS SSA from AERONET SSA below 0.03, the AOD difference needs to be greater than 0.2 to have a high enough signal to noise ratio.

In summary, these sensitivity studies concerning the aerosol model about the real part of aerosol refractive index, AOD dependence of the critical reflectance, and variations of the aerosol SSA

between on the clean day and the polluted day show that the uncertainties of retrieved aerosol SSA caused by these factors are acceptable for a satellite retrieval of aerosol SSA. In addition, to produce retrieval results in good agreement with AERONET measurements, a case need to satisfy two conditions: DZA is smaller than 40 degrees, and the AOD difference between clean day and polluted day is bigger than 0.2.

IV. Algorithm and Validation Strategy

After doing sensitivity studies, we apply the critical reflectance technique on some cases of MODIS data to retrieve aerosol SSA. Our studied regions are dominated by biomass burning aerosols and are collocated with the AERONET sites as follows: Senanga (African savanna), Mongu (African savanna), Mwinilunga (African savanna), and Alta Floresta (Amazon forest). The studied cases are selected based on evaluating MODIS RGB images, MODIS data, and AERONET data to determine that: (1) cloud cover is minimal over the study areas on both the clean day and polluted day, 16 days apart; (2) MODIS DZA is less than 40 degrees; (3) these two days have AOD difference (at 670 nm) greater than or equal to 0.2; and (4) AERONET has level 2 aerosol SSA retrievals available for the polluted day. All retrieval results are validated with collocated AERONET retrieval products, and regional SSA maps are produced.

As discussed in section I, aerosol SSA can be retrieved from the critical reflectance measurements performed with MODIS data as shown in Fig. 1, 2, and 3. Next, as quality control, we have removed cells bearing any of the following properties: (1) having negative critical reflectance; (2) SSA greater than 1 or smaller than 0; (3) an SSA uncertainty derived from robust fitting (DuMouchel & O'Brien, 1989) greater than 0.03; (4) root mean square error (RMSE)

greater than 0.006 between the data points and the fitting results; and (5) the effective path radiance smaller than 0.02 (corresponding to an AOD difference greater than 0.2.

In addition, recent studies have shown that aerosol SSA varies with biomass burning stages and the aerosol aging process (Abel et al., 2003; Zaveri et al., 2010). Therefore, AERONET level 2 aerosol SSA measured at the closest time to the MODIS overpass time is used for the validation, instead of the daily average. In these AERONET level 2 closest time SSA retrievals, the SZA is in the range of 53 degrees to 76 degrees. We compare the AERONET SSA with the mean and the standard deviation of our retrieved aerosol SSA. In order to calculate aerosol SSA variance with less than nine samples, we apply a chi square distribution correction and set a confidence interval of 50% (Bevington, 1969).

According to our quality assurance analysis, accurate biomass burning aerosol SSA can be retrieved with the critical reflectance technique at 0.47, 0.55, and 0.67 μm channels; however, there is not enough signal to noise ratio at the other four aerosol channels (0.86, 1.24, 1.64, and 2.12 μm) to retrieve biomass burning aerosol SSA, i.e., there are no cells left out of nine total after applying our data quality criteria. Next, we validate aerosol SSA retrieved from MODIS data with collocated AERONET measurements (AERONET SSAs at 0.47 and 0.55 μm used here is the 1st order interpolation AERONET SSAs at 0.440 and 0.676 μm).

V. Results

(a) Aerosol SSA Measurements over 60 × 60 km Area

Aerosol SSA was retrieved by applying the algorithm described above, and the result was compared with collocated AERONET measurements in South Africa and South America. According to Fig. 9, approximately one standard deviation (68% by only considering the mean;

88% by considering the mean and the variance) of all the studied cases satisfies the requirement that the absolute difference between MODIS SSA and AERONET SSA is smaller than 0.03. Figure 9 also indicates that aerosol SSA has a larger spatial variation (represented by larger error bars) in South America than in South Africa. Specifically, the mean value of the sample variance is 0.04 for the cases in South America and 0.02 in South Africa.

In addition, the comparison of the mean and sample variance of aerosol SSA over time for each studied locations between MODIS retrievals and AERONET measurements is displayed in Table. 2. According to Table. 2, aerosol SSA retrievals from MODIS are biased lower than AERONET measurements over Mwinilunga, which might be caused by problems in either MODIS or AERONET retrievals. Table 2 also shows that climatologically for the other sites, MODIS retrieval results agree well with AERONET measurements. The biggest difference between MODIS mean and AERONET mean is 0.02. This indicates that aerosol SSA retrieved from MODIS is accurate enough to be used in climatologic studies.

(b) Regional Aerosol SSA Maps

The above validation results show that applying the critical reflectance technique with MODIS data can retrieve aerosol SSA in reasonable agreement with AERONET results within AERONET uncertainty levels. Next, by expanding the studied areas, we produce regional aerosol SSA maps, which have wide applications in climate modeling and radiative forcing calculations. For example, Figure 10 and Figure 11 show aerosol SSA (at 470 nm) maps over South Africa and South America. In addition, the means and the standard deviations (representing the spatial variation) of aerosol SSA at 470, 550, and 670 nm over both regions are listed in Table. 3. Again, these results also indicate that aerosol SSA has a larger spatial

variation in South America than in South Africa, which is in consistent with the results from Fig. 9. The SSA map over the Amazon shows significant connection between the distribution of SSA and AOD. Both results (AOD and SSA) show greater values in the northern part of the Amazon, which is compatible with the particle properties and aerosol loading of forest smoke versus and Cerrado smoke (Dubovik et al., 2002).

VI. Conclusions

In this research, the critical reflectance technique is applied on MODIS data from biomass burning regions by comparing reflectance at TOA in two days (a clean day and a polluted day 16 days apart) to retrieve the aerosol SSA on the polluted day. First, this study describes a method to determine critical reflectance from MODIS data. Second, sensitivity studies that examine a range of aerosol conditions expected for our study areas - about aerosol models, the variation of the real part of aerosol refractive index, AOD dependence of the critical reflectance, and the variation of background aerosol SSA between a clean day and a polluted day – indicate that these factors have manageable effect on the retrieval results. In the mean time, a DZA smaller than 40 degrees and an AOD difference greater than 0.2 are required to provide accurate retrieved aerosol SSA values. We did not test the effect of our assumptions of particle size and shape on retrievals of SSA because the all smoke aerosol is expected to be spherical and with minimal variation in size distribution. Critical reflectance retrievals and subsequent mapping to SSA may show greater sensitivities and uncertainties for other aerosol types and different surfaces. Aerosol mixtures of smoke and dust may be especially difficult.

Validation results show that the retrieved aerosol SSA from MODIS agrees well with collocated AERONET measurements. The ensemble average SSA results from the critical reflectance

techniques are in good agreement with collocated AERONET ensemble averages, within 0.02 in all cases, except for the Mwinilunga station that seems to present some artificial bias. Moreover, the analysis of aerosol SSA from MODIS retrievals concludes that aerosol SSA has a larger spatial variation in South America than in South Africa, and that we can see the South American north-south gradient in SSA and AOD reported by previous studies. Likewise the critical reflectance method also reproduces findings that show African savanna SSA about 0.08 to 0.09 lower than what is measured in the Amazon forest.

However, the power of the critical reflectance method is not in its ability to reproduce previous point measurements or retrievals, either spatially (AERONET) or temporally (field experiments). The true contribution of the critical reflectance method, demonstrated here, is to offer frequent quantitative measures of spectral aerosol SSA over broad regions, and to capture the spatial and temporal variability of this essential particle property.

Acknowledgements. We would like to thank NASA for funding this project with under the grant NNX08AJ78G. We also would like to thank the MODIS team and AERONET team for their excellent work on the instrument development, maintenance, and calibration. We thank their effort on data quality control and providing data to the public as well. Thanks also go to Kelley Wells, Tom Eck, TianLe Yuan, and Ralph Kahn for many helpful comments.

References:

Ackerman, A.S., Toon, O.B., Stevens, D.E., Heymsfield, A.J., Ramanathan, V., & Welton, E.J. (2000). Reduction of Tropical Cloudiness by soot. *Science*, Vol. 288, No. 5468, pp. 1042-1047.

Ackerman,T.P., & Toon,O.B. (1981). Absorption of visible radiation in atmosphere containing mixtures of absorbing and nonabsorbing particles. *Applied Optics*, Vol. 20, No. 20, pp. 3661-3668.

Atwater,M.A. (1970). Planetary Albedo Changes Due to Aerosols, *Science*, Vol. 170, No 3953, pp. 64-66.

Bevington, P.R. (1969). Data reduction and error analysis for the physical sciences. New York: McGraw-Hill.

Bond, T. C., Anderson,T. L., & Campbell,D. (1999) Calibration and inter comparison of filter-based measurements of visible light absorption by aerosols, *Aerosol Sci Tech*, Vol. 30, pp. 582-600.

Clarke, A.D., Noone, K.J., Heintzenberg, J., Warren,S.G., & Covert.D.S. (1987).Aerosol light absorption measurement techniques: analysis and intercomparisons. *Atmospheric Environment*, Vol. 21, No. 6, pp. 1455-1465.

Davidi,A., Koren, I., & Remer, L. (2009). Direct measurements of the effect of biomass burning over the Amazon on the atmospheric temperature profile. *ACPD*, Vol. 9, pp. 12007-12025.

Dubovik O, Holben, B.O., Lapyonok, T., Sinyuk, A, Mishchenko, I, Yang, P., et al (2002). Non spherical aerosol retrieval method employing light scattering by spheroids. *Geophys Res Lett*, Vol. 29, NO. 10, 10.1029/2001GL014506

Dubovik,O., Holben, B.N., Kaufman, Y.J., Yamasoe, M., Smirnov,A., & Tanre,D., ey al. (1998). Single-scattering albedo of smoke retrieved from the sky radiance and solar transmittance measured from ground. *J. Geophys. Res.*, Vol. 103, No. D24, pp. 31,903-31,923.

DuMouchel, W. H., & F. L. O'Brien (1989). Integrating a robust option into a multiple regression computing environment. *Computer Science and Statistics*: *Proceedings of the 21st Symposium on the Interface*. Alexandria, VA: American Statistical Association.

Feingold,G., Jiang,H., & Harrington, J.Y. (2005). On smoke suppression of clouds in Amazonia, *Geophys Res Lett*, Vol.32, L02804, doi: 10.1029/2004GL021369.

Fraser,R.S. & Kaufman, Y. J. (1985). The relative importance of Aerosol Scattering and Aabsorption in Remote Sensing. *IEEE TRANSACTIONS ON GEOSCIENCE AND REMOTE SENSING*, Vol. GE-23, No.5, pp. 625-633.

Hansen, A.D.A., Rosen, H., & Novakov, T. (1984). The aethalometer-an instrument for the real - time measurement of optical absorption by aerosol particles. *Sci Total Environ*, Vol.36, pp. 191-196.

Hansen,J., Sato,M., Ruedy, R., Lacis, A., & Oinas, V. (2000). Global warming in the twenty-first century: an alternative scenario. *PNAS*, Vol. 97, Part. 18, pp 9875-9880.

Herman,R.J.,Bhartia,K.P., Torres,O., Hsu,C., Seftor,C., & Celarier,E. (1997). Global distribution of UV-absorbing aerosols from Nimbus 7/TOMS data. *J. Geophys. Res*., Vol. 102, No. D14, pp. 16911-16922.

Hsu, N. C., J. R. Herman, and C. Weaver (2000), Determination of radiative forcing of Saharan dust using combined TOMS and ERBE data, *J. Geophys. Res.*, 105(D16), 20,649-20,661.

Hu, R.M., Martins, R.V., & Fairlie, T.D. (2007). Global retrieval of columnar aerosol single scattering albedo from space-based observations. *J. Geophys. Res*., Vol. 112, D02204, doi: 10.1029/2005JD006832.

Hu, R.M., Sokhi, R.S., & Fisher, B.E.A. (2009). New algorithms and their application for satellite remote sensing of surface PM2.5 and aerosol absorption. *Aerosol Science*, Vol. 40, pp. 394-402.

Ichoku, C., Remer, L.A., Kaufman, Y.J., Levy, R., Chu,D.A., & Tanre, D., et al. (2003). MODIS observation of aerosols and estimation of aerosol radiative forcing over southern Africa during SAFARI 2000. *J. Geophys. Res*., Vol. 108, No. D13, pp. 8499-8511.

Jeong, M-J., & Hsu, N. C. (2008). Retrievals of aerosol single-scattering albedo and effective aerosol layer height for biomass-burning smoke: Synergy derived from ""A-Train"" sensors. *Geophys Res Lett*, Vol. 35, L24801, doi: 10.1029/2008GL036279.

Kalashnikova, O.V., Kahn, R., Sokolik, I.N., & Li,W-H. (2005). Ability of multiangle remote sensing observations to identify and distinguish mineral dust types: Optical models and retrievals of optically thick plumes. *J. Geophys. Res*., Vol. 110, D18S14, doi:10.1029/2004JD004550.

Kalashnikova, O.V., & Kahn, R., (2006). Ability of multiangle remote sensing observations to identify and distinguish mineral dust types: 2. Sensitivity over dark water. *J. Geophys. Res*., Vol. 111, D11207, doi:10.1029/2005JD006756.

Mishchenko, M.I., Cairns, B., Kopp, G., Schueler,C.F., Fafaul, B.A., & Hansen,J.E., et al. (2007). Accurate Monitoring of Terrestrial Aerosols and Total Solar Irradiance- Introducing the Glory Mission. *American Meteorological Society*, pp. 677-691.

Kaufman, Y. J. (1987). Satellite Sensing of Aerosol Absorption. *Journal of Geophysical Research*, Vol. 92, No.D4, pp. 4307-4317.

Kaufman,Y.J., Tucker, C.J., & Fung,I. (1990). Satellite Measurements of Large-Scale Air Pollution:Methods. *J. Geophys. Res*., Vol. 95, No.D7, pp. 9927-9939.

Kaufman,Y.J., Tanre,D., Dubovik, O., Karnieli, & Remer,L.A. (2001).Absorption of sunlight by dust as inferred from satellite and ground-based remote sensing. *Geophys Res Lett*, Vol. 28, No. 8, pp. 1479-1482.

Kaufman,Y.J., Tanre,D., & Boucher,O. (2002). A satellite view of aerosols in the climate system. *Nature*, Vol 419, pp. 215-223.

Koren,I., Kaufman,Y.J., Remer,L.A., & Martins,J,V. (2004). Measurements of the effect of Amazon Smoke on inhibition of Cloud Formation. *Science*, Vol. 303, No. 5662, pp. 1342-1345.

Koren,I., Martins,J,V., Remer,L.A., & Afargan, H. (2008). Smoke invigoration versus inhibition of clouds over the Amazon. *Science*, Vol. 321, pp. 946-949.

Martins, J. V., Artaxo, P., Liousse, C., Reid, J. S., Hobbs, P. V., & Kaufman Y. J. (1998), Effects of black carbon content, particle size, and mixing on light absorption by aerosols from biomass burning in Brazil, *J. Geophys. Res.*, 103(D24), 32,041–32,050, doi:10.1029/98JD02593.

Martins, J. V., Didier, T., Remer, L., Kaufman,Y, Mattoo, S., & Levy, R., (2002). MODIS cloud screening for remote sensing of aerosols over oceans using spatial variability : First result and evaluation of aerosol from the Terra Spacecraft (MODIS). *Geophys Res Lett*, Vol. 29, No. 12, 10.1029/2001GL013252.

Martins, J. V., Artaxo,P., Kaufman,Y.J., Castanho, A.D., & Remer,L.A. (2009). Spectral absorption properties of aerosol particles from 350-2500nm. *Geophys Res Lett*, Vol. 36, L13810.

McComiskey, S. E. Schwartz, B. Schmid, H. Guan, E. R. Lewis, P. Ricchiazzi, and J. A. Ogren (2008), Direct aerosol forcing: Calculation from observables and sensitivities to inputs, J. Geophys. Res., 113, D09202, doi:10.1029/2007JD009170.

Mitchell, JM.JR. (1971). The Effect of Atmospheric Aerosols on Climate with Special Reference to Temperature near Earth's surface. *Journal of Applied Meteorology*, Vol. 10, Issue. 4, pp. 703-714.

Moosmuller, H., Chakrabarty,P.K., & Arnott,W.P. (2009). Aerosol Absorption and its measurement: A review. *Journal of Quantitative Spectroscopy and Radiative Transfer*, Vol.110, issue. 11, pp. 844-878.

Penner, J.E., Dickinson,E.R., & O'Neill, A.C. (1992). Effects of aerosol from Biomass burning on the global radiation budget. *Science*, Vol.256, No.5062, pp. 1432-1434.

Ramana,M.V. & Ramanathan,V. (2006). Abrupt transition from natural to anthropogenic aerosol radiative forcing: observations at the ABC-Maldives Climate Observatory. *J. Geophys. Res*., Vol. 111, D20207, doi:10.1029/2006JD007063

Ramanathan, V., Ramana,M.V., Roberts, G., Kim, D., Corrigan, C., & Chung, C., et al. (2007). *Nature*, Vol. 448, pp. 575-579.

Ramanthan, V., Chung, C., Kim, D., Bettge,T., Buja,L., & Kiehl,J.T., et al. (2005). Atmospheric brown clouds: impacts on South Asian climate and hydrological cycle. *PNAS*, Vol. 102, No. 15, pp. 5326- 5333.

Ramanthan, V., Crutzen, P.J., Kiehl,J.T., & Rosenfeld, D. (2001) . Aerosols,climate,and the hyfrological cycle. *Science*, Vol. 294, pp. 2119-2124.

Reid, J. S., Hobbs, P. V., Liousse, C., Martins, J. V., Weiss, R. E., & Eck, T. F.(1998). Comparisons of techniques for measuring shortwave absorption and black carbon content of aerosols from biomass burning in Brazil, *J. Geophys. Res*., 103(D24), pp. 32,031-32,040.

Satheesh, S. K., Torres,O., Remer,L.A., Babu,S.S., Vinoj, V. & Eck,T.F., et al. (2009). Improved assessment of aerosol absorption using OMI-MODIS joint retrieval, *J. Geophys. Res.*, Vol. 114, D05209, doi:10.1029/2008JD011024.

Sato, M., Hansen,J., Koch,D., Lacis,A., Ruedy, R., & Dubovik, O, et al. (2003). Global atmospheric black carbon inferred from AERONET. *PNAS*, Vol. 100, No. 11, pp. 6319-6324.

488 Torres, O., P. K. Bhartia, J. R. Herman, Z. Ahmad, and J. Gleason (1998), Derivation of aerosol
489 properties from satellite measurements of backscattered ultraviolet radiation: Theoretical basis, *J.*
490 *Geophys. Res.*, 103(D14), 17,099-17,110.
491 Wang, C. (2004). A modeling study on the climate impacts of black carbon aerosols. *J. Geophys.*
492 *Res*., Vol. 109, D03106, doi: 10.1029/2003JD004084.
493 Zhu, A, V.Ramanathan, F.Li & D.Kim (2007), Dust plumes over the Pacific, Indian, and
494 Atlantic oceans: Climatology and radiative impact, *J.Geophys.Res*., 112, D16208,
495 doi:10.1029/2007JD008427.

Figure captions:

FIG.1. MODIS RGB images over Africa. The image on the left is for Julian day 266 of year 2000 (clean day), and the blue color box in it represents the 60 × 60 km region around the AERONET site Mongu. Likewise, the image on the right is for day 250 of year 2000 (polluted day), and the purple color box represents the same 60 × 60 km region as the blue color box on the left image. The blue color box and purple color box are used respectively to contrast the clean day and the polluted day.

FIG.2. Projected apparent reflectance for the polluted and clean day at 670 nm after applying a common cloud mask to both days. The image on the left shows the reflectance in the blue color box in Fig.1 with an average AOD (at 670 nm) =0.36. The image on the right shows the reflectance in the purple color box in Fig.1 with an averaged AOD (at 670 nm) =0.7. The color bar represents the apparent reflectance.

FIG.3. This figure demonstrates how to calculate critical reflectance using MODIS data from two days. The blue dots are the scatter plot of the reflectance from the first cell (20 × 20 km range) on the polluted day (the y-axis) versus that on the clean day (the x-axis). The red color line represents the robust fit of the data. The black color line represents y=x, when reflectance (at the TOA) on the clean day equals reflectance (at the TOA) on the polluted day. The reflectance value at the crossing point (as shown by the arrows in the figure) between the black color line and the red color line is defined as "critical reflectance". The intercept of the fitted red color line on the y- axis is defined as "effective path radiance".

FIG.4. Sensitivity study for the variation of the real part of aerosol refractive index. The x- axis represents the real part of the refractive index, and the y-axis represents aerosol SSA calculated

518 from Mie theory. The real refractive index as 1.49, the imaginary refractive index as 0.024, and
519 the input size distribution are from AERONET retrieval results over Mongu on day 250 in year
520 2000. This result shows that an uncertainty of real part of aerosol refractive index of 2.3% leads
521 to an SSA uncertainty of 0.01, 0.017, and 0.021 when the imaginary refractive index is 0.012,
522 0.024, and 0.036 respectively.

523 **FIG.5**. This figure shows the AOD dependence of the critical reflectance. The x-axis represents
524 AOD (at 670 nm) on a polluted day, and the y- axis represents the calculated critical reflectance
525 for AOD values (at 670 nm; on a clean day) of 0.1 (red solid line), 0.2 (green solid line), and 0.3
526 (continued light blue line). The simulations use the following conditions: solar zenith angle
527 (SZA)=26.8 degrees, solar azimuth angle (SAZA)=37.77 degrees, detector zenith angle
528 (DZA)=38.65 degrees, user azimuth angle (phi)=277.38 degrees, wavelength=0.67 μm, and
529 SSA=0.8. When AOD on the clean day varies from 0.1 to 0.3, the variation of critical reflectance
530 is 0.005 (AOD of 0.5 on polluted day) and 0.003 (AOD of 1 on polluted day). In addition, when
531 AOD on the polluted day varies from 0.5 to 1, the variation of critical reflectance is 0.01(AOD of
532 0.1 on the clean day).

533 **FIG.6**. The sensitivity study of aerosol SSA (at 670 nm) to varying critical reflectance. The x-
534 axis represents SSA, and the y-axis represents critical reflectance. The green curve shows the
535 unique correlation between critical reflectance and SSA. AOD on the clean (polluted day) day is
536 0.2 (0.7). It shows that the critical reflectance uncertainty of 0.01 leads to an SSA uncertainty of
537 0.025 (when SSA=0.8). Similarly, a critical reflectance uncertainty of 0.028 causes an SSA total
538 uncertainty of 0.01 (when SSA=0.95).

FIG.7. This figure demonstrates that DZA affects aerosol SSA retrievals. The x-axis represents DZA for each case, and the y-axis represents the absolute difference between the retrieved aerosol SSA (over Senanga in 2000) from MODIS on *TERRA* and AERONET level 2 daily-averaged aerosol SSA. The red color bar over each data point represents the AERONET SSA uncertainty of 0.03. The result indicates that the difference between aerosol SSA retrieved from MODIS and from AERONET increases as DZA increases. This effect is likely caused by the simplified assumption of a Lambertian surface reflectance in the radiative transfer simulations.

FIG.8. This figure demonstrates that AOD differences affect aerosol SSA retrievals. The x-axis represents the AOD difference at 670 nm between the clean day and the polluted day, and the y-axis represents the absolute difference between aerosol SSA (over Mongu in 2000) retrieved from MODIS and AERONET level 2 daily-averaged aerosol SSA. The result shows that AOD difference needs to be greater than 0.2 in order to produce a high enough signal to noise ratio and to keep the deviation of MOIDS SSA from AERONET SSA below 0.03.

FIG.9. Comparison of aerosol SSA retrieved from MODIS with collocated AERONET measurement in South Africa (plots on the left) and South America (plots on the right). The x-axis represents the case numbers, and the y-axis represents the difference between aerosol SSA from AERONET and from MODIS. In addition, bars over each data point represent SSA variance (among the remaining cells in 60 $\times$ 60 km range) at a 50% of confidence interval and with a chi square distribution correction. Since AERONET SSA has an uncertainty of 0.03, the aerosol SSA retrieved from MODIS agrees well with AERONET measurements (68% by only considering the mean; 88% by considering the mean and the variance), i.e., the absolute difference between aerosol SSA from AERONET and MODIS is smaller than 0.03. The result also shows that aerosol SSA has a larger spatial variation in South America than in South Africa.

562 **FIG. 10**. Regional AOD and aerosol SSA (at 470 nm) maps. The figures on the left represent the
563 region over South Africa with latitude = [-15 to -11] and longitude = [21 to 25] on day 254 in
564 2000 (day 238 as the clean day). The figures on the right represent the region over South
565 America with latitude = [-12 to -8] and longitude = [-60 to -56] on day 241 in 2006 (with 225 as
566 the clean day). Both images have a resolution of 20×20 km.

567 **FIG. 11**. Regional AOD and aerosol SSA (at 470 nm) maps. The figures on the left represent the
568 region over South Africa with latitude = [-18 to -14] and longitude = [22 to 26] on day 250 in
569 2000 (day 266 as the clean day). The figures on the right represent the region over South
570 America with latitude = [-16 to -12] and longitude = [-60 to -56] on day 252 in 2004 (with 268 as
571 the clean day). Both images have a resolution of 20×20 km.

572

Table. 1. Sensitivity study for varying aerosol SSA between the clean day and the polluted day. Wavelength = 0.67 μm; AOD (on clean day) = 0.2; AOD (on polluted day) = 0.7; SZA = 26.8º; SAZA = 37.77º; DZA = 38.65º; DAZA = 277.38º; Real part of the refractive index = 1.51. The first (last) four rows in the first column represents aerosol SSA on polluted day as a constant 0.898 (0.972); the second column represents varying aerosol SSA on clean day; the third column represents the simulated critical reflectance; the fourth column represents the retrieved aerosol SSA; and the last column is the difference between the retrieved aerosol SSA and the real aerosol SSA on the polluted day. The results show that the uncertainty caused by varying aerosol SSA between the clean day and the polluted day is acceptable.

584

SSA (on polluted day)	SSA (on clean day)	Critical reflectance	SSA (Retrieved)	SSA (retrieved) – SSA (polluted day)
0.898	0.986	0.205	0.872	-0.026
	0.934	0.226	0.887	-0.011
	0.855	0.263	0.909	0.011
	0.824	0.281	0.917	0.019
0.972	0.993	0.461	0.966	-0.006
	0.986	0.473	0.968	-0.004
	0.934	0.601	0.983	0.011
	0.910	0.691	0.990	0.018

585

586

Table 2. The mean and sample variance of aerosol SSA from MODIS retrievals and AERONET measurements over different locations. The table shows that MODIS retrievals are biased smaller than AERONET measurements over Mwinilunga, which might be caused by either problems in MODIS or in the AERONET retrievals. Over other sites, the maximum difference between MODIS SSA and AERONET SSA is 0.02. This high accuracy aerosol SSA retrievals from MODIS indicates its promising application in climatological studies over a given region.

AERONET sites	SSA (at 470 nm)		SSA (at 550 nm)		SSA (at 670 nm)	
	AERONET	MODIS	AERONET	MODIS	AERONET	MODIS
Alta Floresta	0.92 ± 0.02 (22 cases)	0.92 ± 0.03	0.91 ± 0.03 (22 cases)	0.92 ± 0.03	0.92 ± 0.03 (18 cases)	0.90 ± 0.03
Senanga	0.86 ± 0.01 (7 cases)	0.87 ± 0.01	0.85 ± 0.01 (7 cases)	0.87 ± 0.01	0.84 ± 0.01 (7 cases)	0.86 ± 0.01
Mongu	0.88 ± 0.02 (14 cases)	0.86 ± 0.02	0.87 ± 0.03 (14 cases)	0.86 ± 0.02	0.86 ± 0.03 (14 cases)	0.84 ± 0.02
Mwinilunga	0.90 ± 0.02 (3 cases)	0.86 ± 0.01	0.90 ± 0.02 (3 cases)	0.85 ± 0.01	0.89 ± 0.03 (3 cases)	0.84 ± 0.01

596 Table 3. This table shows the mean and the standard deviation of aerosol SSA at 470, 550, and
597 670 nm for the same cases as shown in SSA maps in Fig. 10 and Fig. 11. The data in the table
598 shows aerosol SSA has a larger spatial variation in South America than in South Africa, which is
599 consistent with the result from Fig.9.

600

Case Information	Aerosol SSA: mean ± standard deviation		
	470 nm	550 nm	670 nm
latitude = [-15 to -11]; longitude = [21 to 25] over South Africa; on day 254 in 2000	0.86 ± 0.02	0.84 ± 0.02	0.82 ± 0.02
latitude=[-18 to -14]; longitude=[22 to 26] over South Africa; on day 250 in 2000	0.86 ± 0.02	0.84 ± 0.02	0.81 ± 0.02
latitude =[-12 to -8]; longitude = [-60 t0 -56] over South America; on day 241 in 2006	0.90 ± 0.03	0.90 ± 0.03	0.87 ± 0.04
latitude=[-16 to -12]; longitude=[-60 to -56] over South America; on day 252 in 2004	0.91 ± 0.04	0.92 ± 0.03	0.91 ± 0.03

601

602

FIG.1. MODIS RGB images over Africa. The image on the left is for Julian day 266 of year 2000 (clean day), and the blue color box in it represents the 60 × 60 km region around the AERONET site Mongu. Likewise, the image on the right is for day 250 of year 2000 (polluted day), and the purple color box represents the same 60 × 60 km region as the blue color box on the left image. The blue color box and purple color box are used respectively to contrast the clean day and the polluted day.

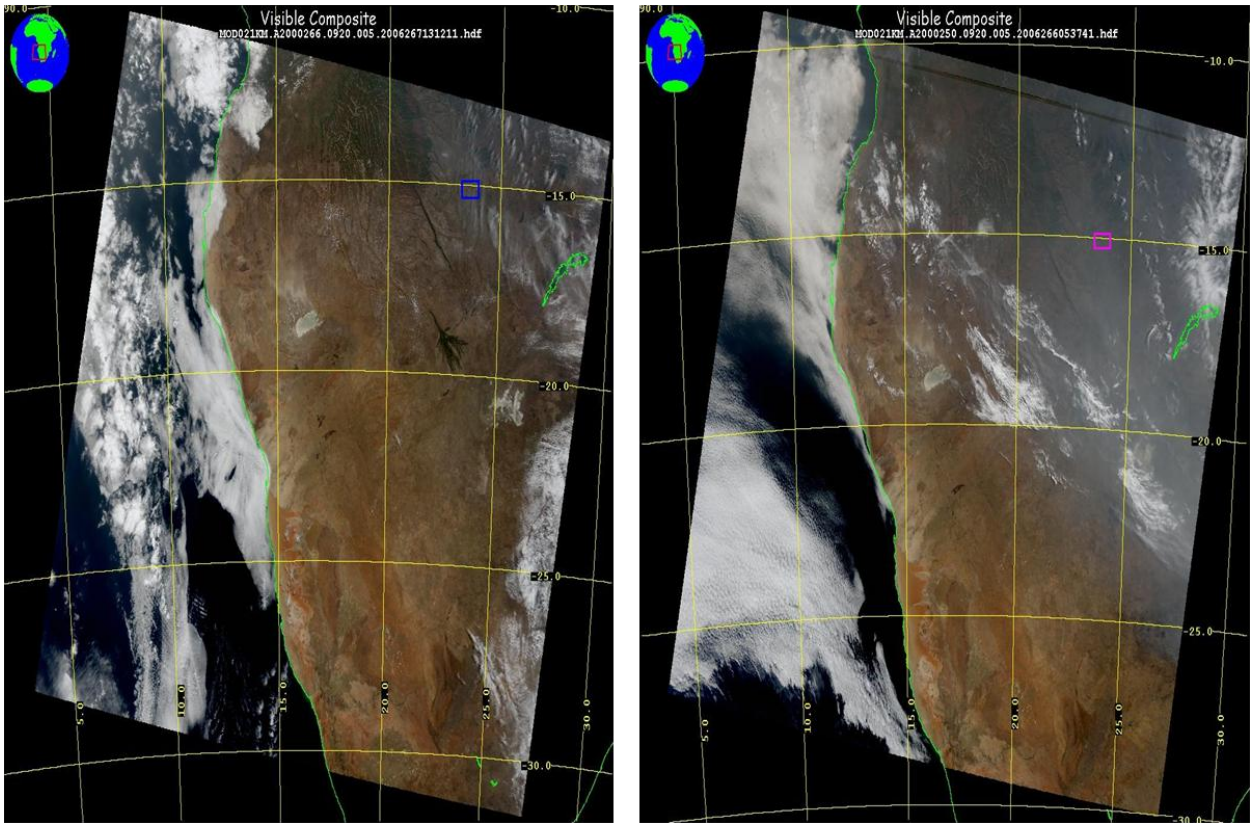

FIG.2. Projected apparent reflectance for the polluted and clean day at 670 nm after applying a common cloud mask to both days. The image on the left shows the reflectance in the blue color box in Fig.1 with an average AOD (at 670 nm) =0.36. The image on the right shows the reflectance in the purple color box in Fig.1 with an averaged AOD (at 670 nm) =0.7. The color bar represents the apparent reflectance.

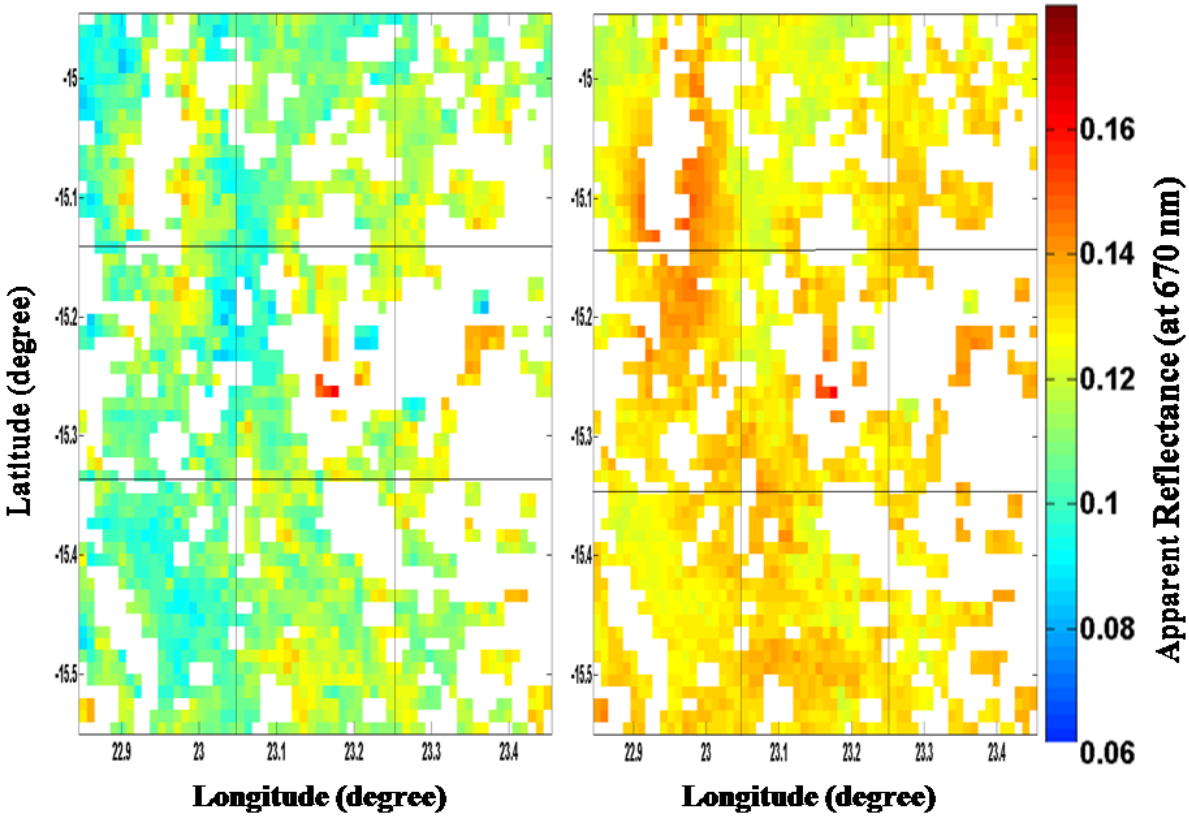

FIG.3. This figure demonstrates how to calculate critical reflectance using MODIS data from two days. The blue dots are the scatter plot of the reflectance from the first cell (20 × 20 km range) on the polluted day (the y-axis) versus that on the clean day (the x-axis). The red color line represents the robust fit of the data. The black color line represents y=x, when reflectance (at the TOA) on the clean day equals reflectance (at the TOA) on the polluted day. The reflectance value at the crossing point (as shown by the arrows in the figure) between the black color line and the red color line is defined as "critical reflectance". The intercept of the fitted red color line on the y- axis is defined as "effective path radiance".

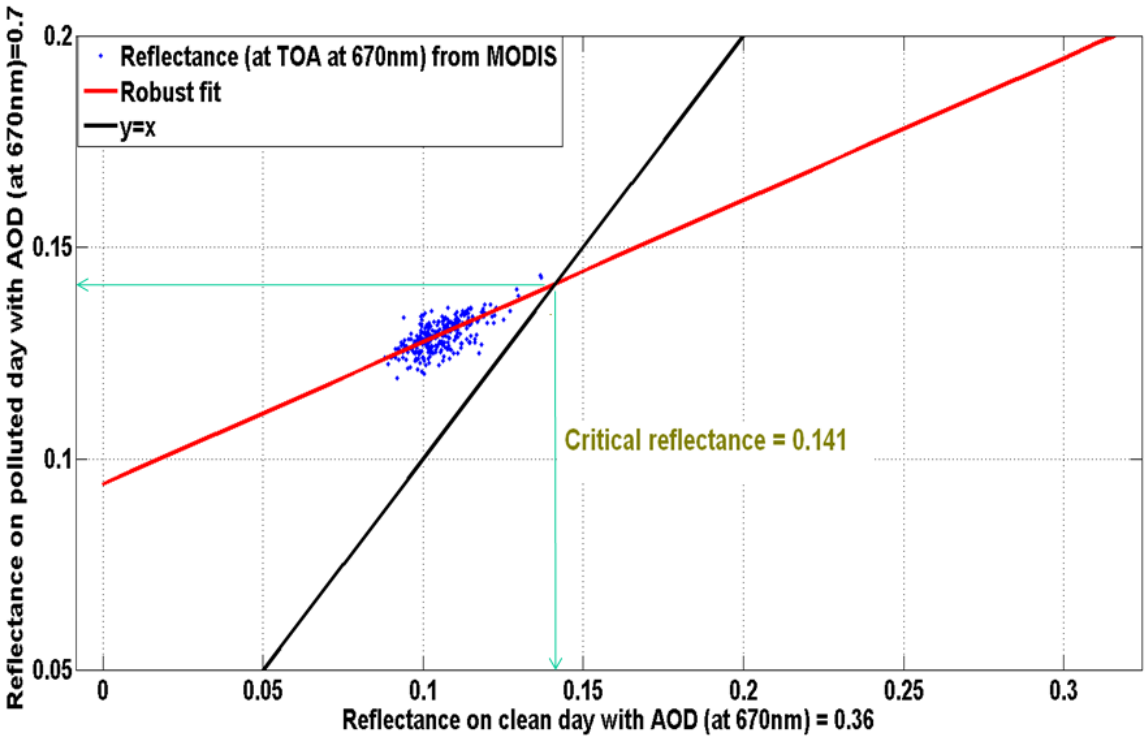

FIG.4. Sensitivity study for the variation of the real part of aerosol refractive index. The x- axis represents the real part of the refractive index, and the y-axis represents aerosol SSA calculated from Mie theory. The real refractive index as 1.49, the imaginary refractive index as 0.024, and the input size distribution are from AERONET retrieval results over Mongu on day 250 in year 2000. This result shows that an uncertainty of real part of aerosol refractive index of 2.3% leads to an SSA uncertainty of 0.01, 0.017, and 0.021 when the imaginary refractive index is 0.012, 0.024, and 0.036 respectively.

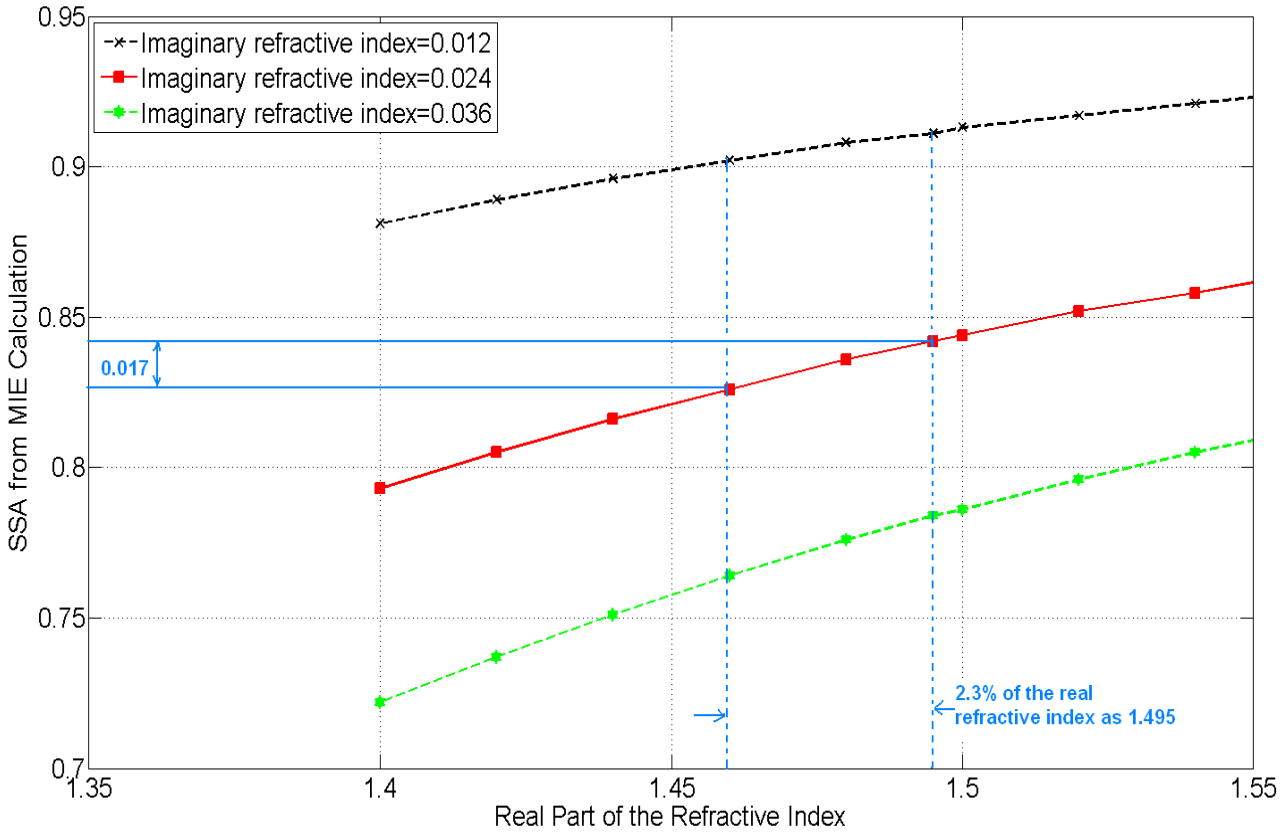

FIG.5. This figure shows the AOD dependence of the critical reflectance. The x-axis represents AOD (at 670 nm) on a polluted day, and the y- axis represents the calculated critical reflectance for AOD values (at 670 nm; on a clean day) of 0.1 (red solid line), 0.2 (green solid line), and 0.3 (continued light blue line). The simulations use the following conditions: solar zenith angle (SZA)=26.8 degrees, solar azimuth angle (SAZA)=37.77 degrees, detector zenith angle (DZA)=38.65 degrees, user azimuth angle (phi)=277.38 degrees, wavelength=0.67 µm, and SSA=0.8. When AOD on the clean day varies from 0.1 to 0.3, the variation of critical reflectance is 0.005 (AOD of 0.5 on polluted day) and 0.003 (AOD of 1 on polluted day). In addition, when AOD on the polluted day varies from 0.5 to 1, the variation of critical reflectance is 0.01(AOD of 0.1 on the clean day).

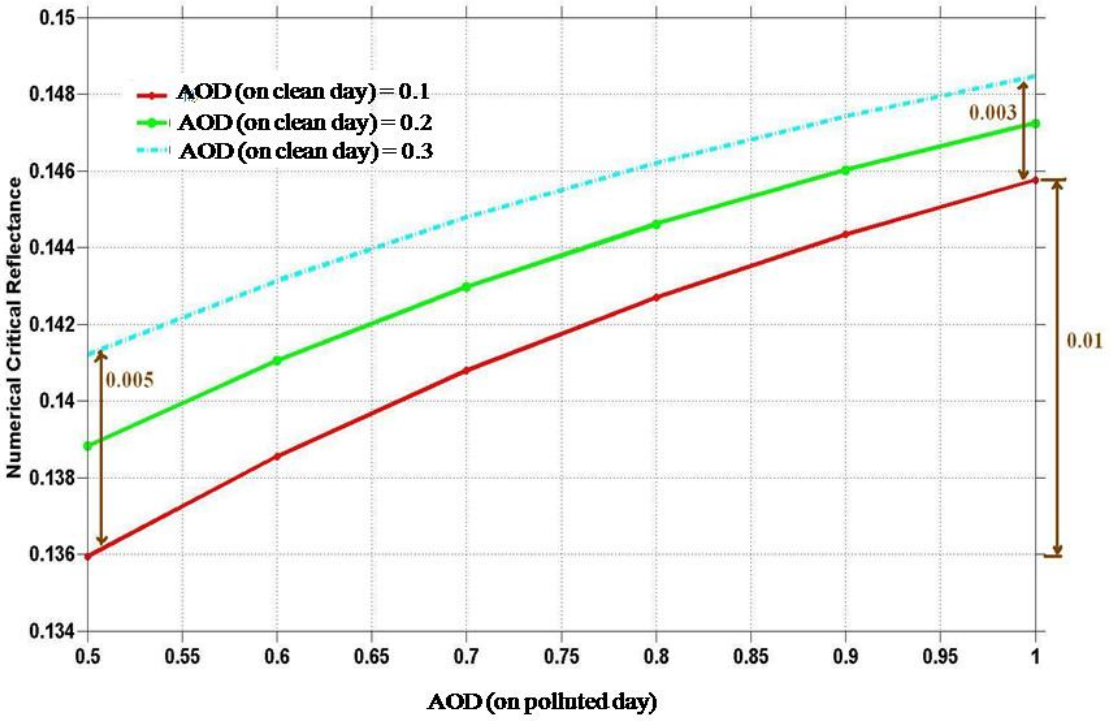

FIG.6. The sensitivity study of aerosol SSA (at 670 nm) to varying critical reflectance. The x-axis represents SSA, and the y-axis represents critical reflectance. The green curve shows the unique correlation between critical reflectance and SSA. AOD on the clean (polluted day) day is 0.2 (0.7). It shows that the critical reflectance uncertainty of 0.01 leads to an SSA uncertainty of 0.025 (when SSA=0.8). Similarly, a critical reflectance uncertainty of 0.028 causes an SSA total uncertainty of 0.01 (when SSA=0.95).

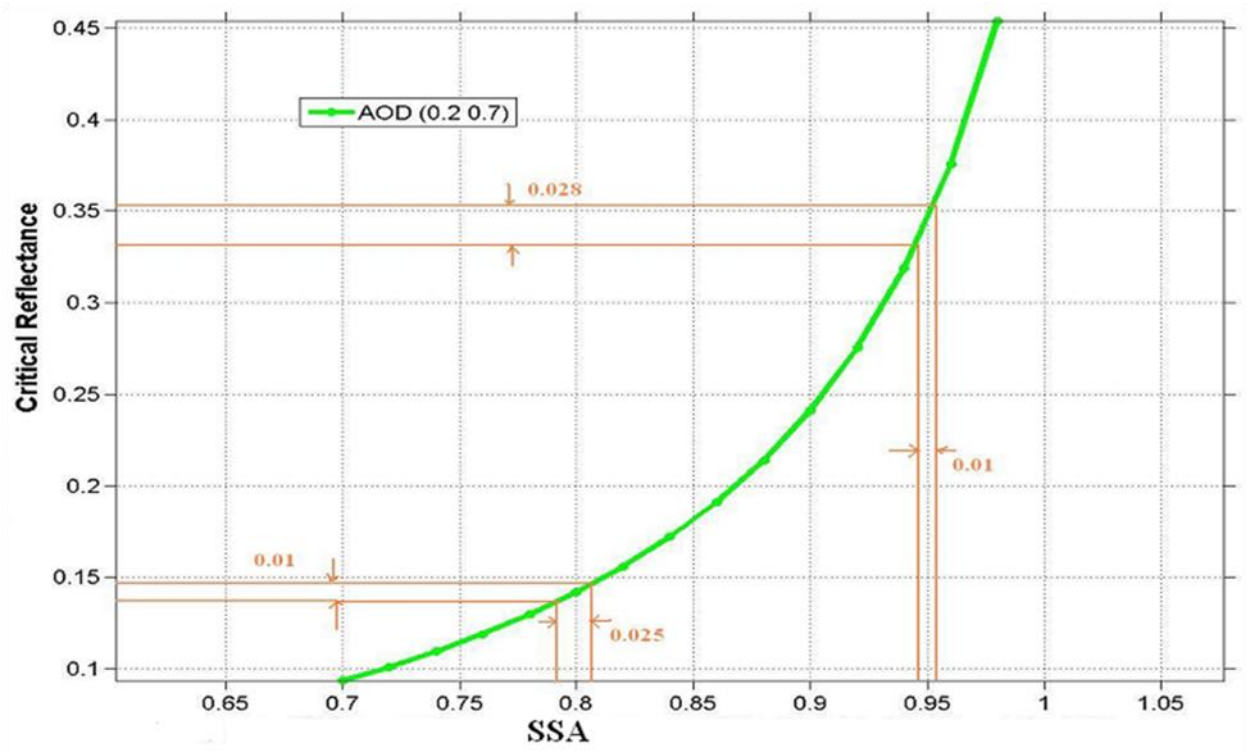

660 FIG.7. This figure demonstrates that DZA affects aerosol SSA retrievals. The x-axis represents
661 DZA for each case, and the y-axis represents the absolute difference between the retrieved
662 aerosol SSA (over Senanga in 2000) from MODIS on *TERRA* and AERONET level 2 daily-
663 averaged aerosol SSA. The red color bar over each data point represents the AERONET SSA
664 uncertainty of 0.03. The result indicates that the difference between aerosol SSA retrieved from
665 MODIS and from AERONET increases as DZA increases. This effect is likely caused by the
666 simplified assumption of a Lambertian surface reflectance in the radiative transfer simulations.

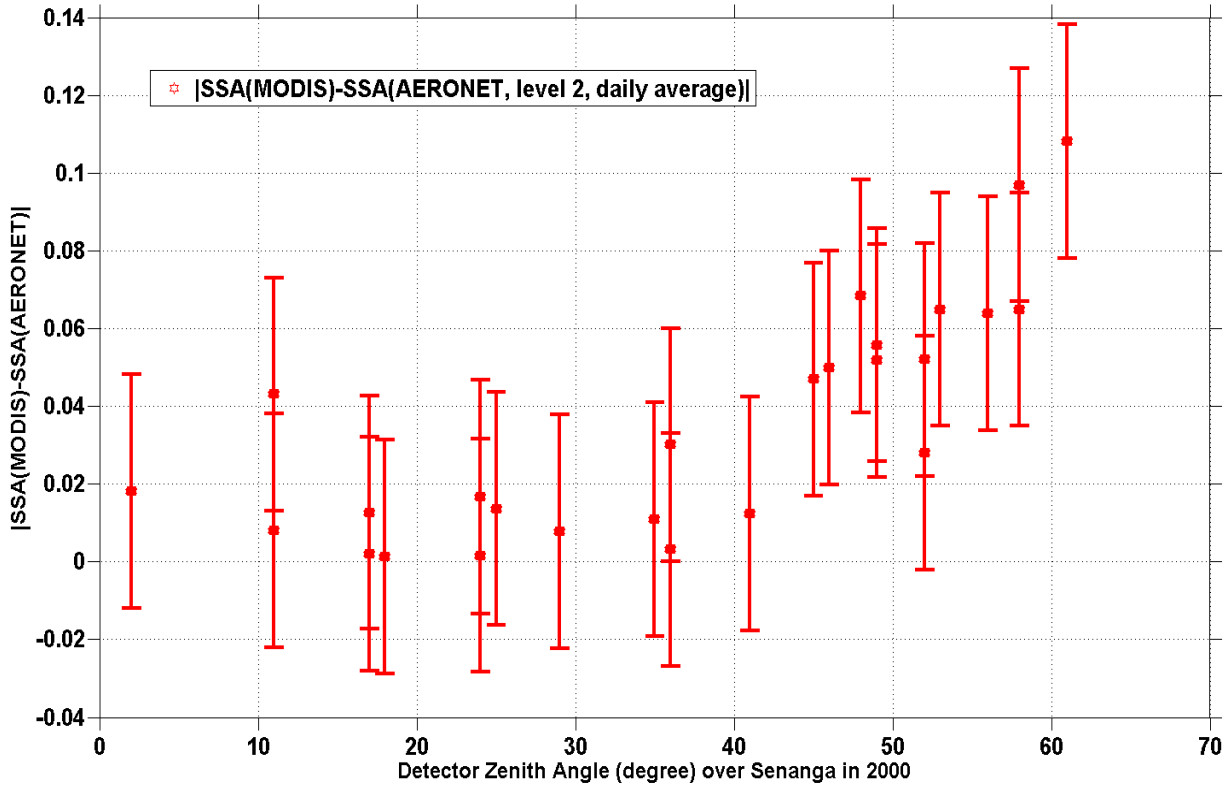

667

668

669 FIG.8. This figure demonstrates that AOD differences affect aerosol SSA retrievals. The x-axis
670 represents the AOD difference at 670 nm between the clean day and the polluted day, and the y-
671 axis represents the absolute difference between aerosol SSA (over Mongu in 2000) retrieved
672 from MODIS and AERONET level 2 daily-averaged aerosol SSA. The result shows that AOD
673 difference needs to be greater than 0.2 in order to produce a high enough signal to noise ratio and
674 to keep the deviation of MOIDS SSA from AERONET SSA below 0.03.

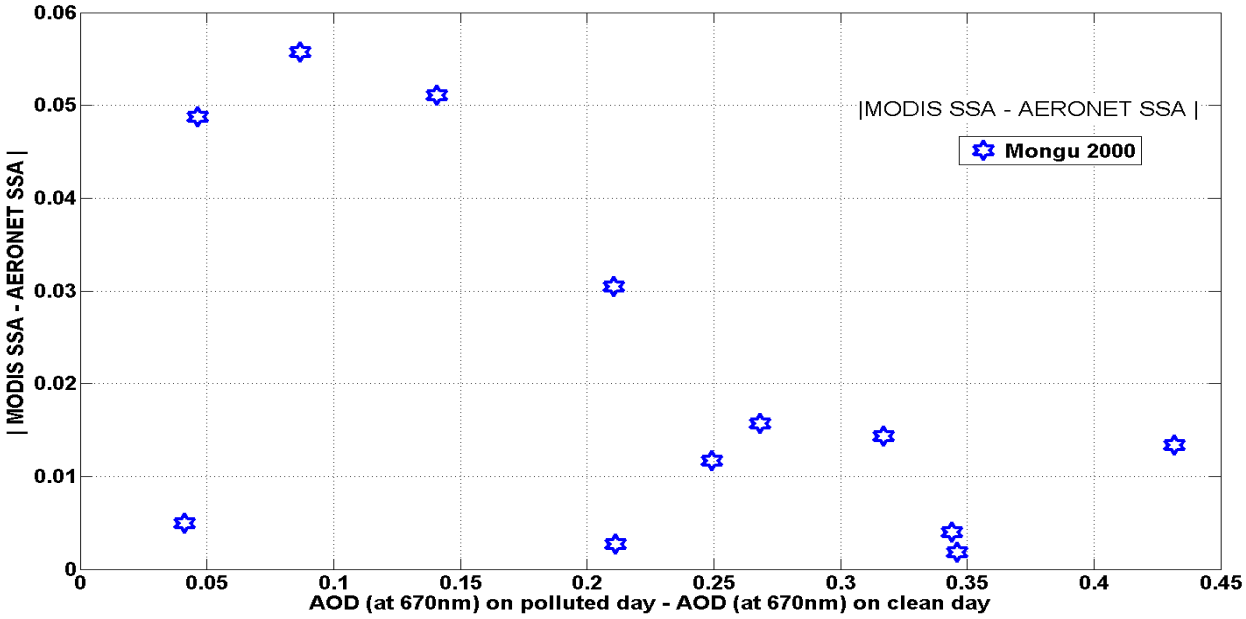

675

676

FIG.9. Comparison of aerosol SSA retrieved from MODIS with collocated AERONET measurement in South Africa (plots on the left) and South America (plots on the right). The x-axis represents the case numbers, and the y-axis represents the difference between aerosol SSA from AERONET and from MODIS. In addition, bars over each data point represent SSA variance (among the remaining cells in 60 × 60 km range) at a 50% of confidence interval and with a chi square distribution correction. Since AERONET SSA has an uncertainty of 0.03, the aerosol SSA retrieved from MODIS agrees well with AERONET measurements (68% by only considering the mean; 88% by considering the mean and the variance), i.e., the absolute difference between aerosol SSA from AERONET and MODIS is smaller than 0.03. The result also shows that aerosol SSA has a larger spatial variation in South America than in South Africa.

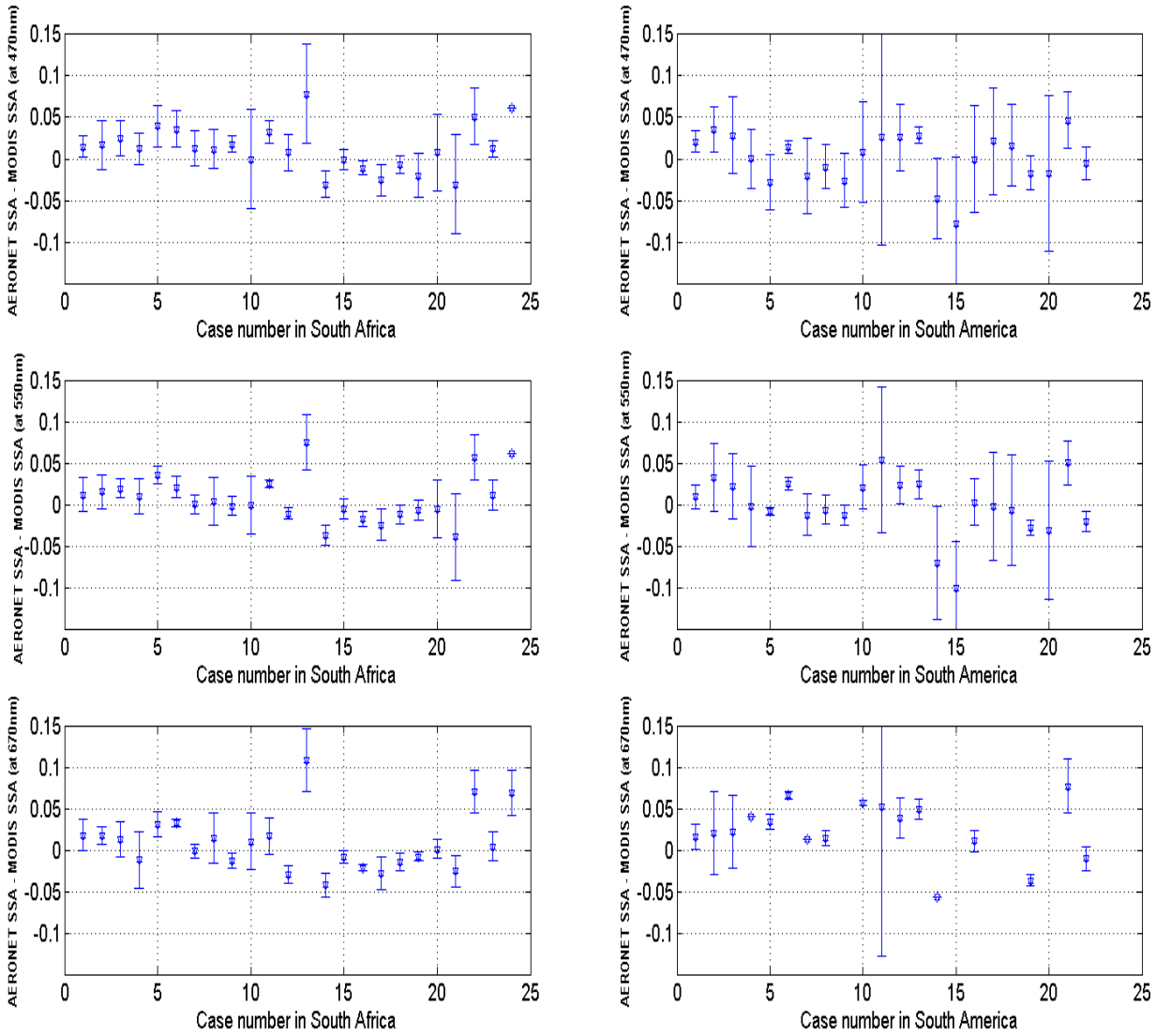
AERONET SSA - MODIS SSA (at 470nm)
AERONET SSA - MODIS SSA (at 550nm)
AERONET SSA - MODIS SSA (at 670nm)
Case number in South Africa
Case number in South America
0.15
0.1
0.05
0
-0.05
-0.1
0
5
10
15
20
25

687

688

FIG. 10. Regional AOD and aerosol SSA (at 470 nm) maps. The figures on the left represent the region over South Africa with latitude = [-15 to -11] and longitude = [21 to 25] on day 254 in 2000 (day 238 as the clean day). The figures on the right represent the region over South America with latitude = [-12 to -8] and longitude = [-60 to -56] on day 241 in 2006 (with 225 as the clean day). Both images have a resolution of 20 × 20 km.

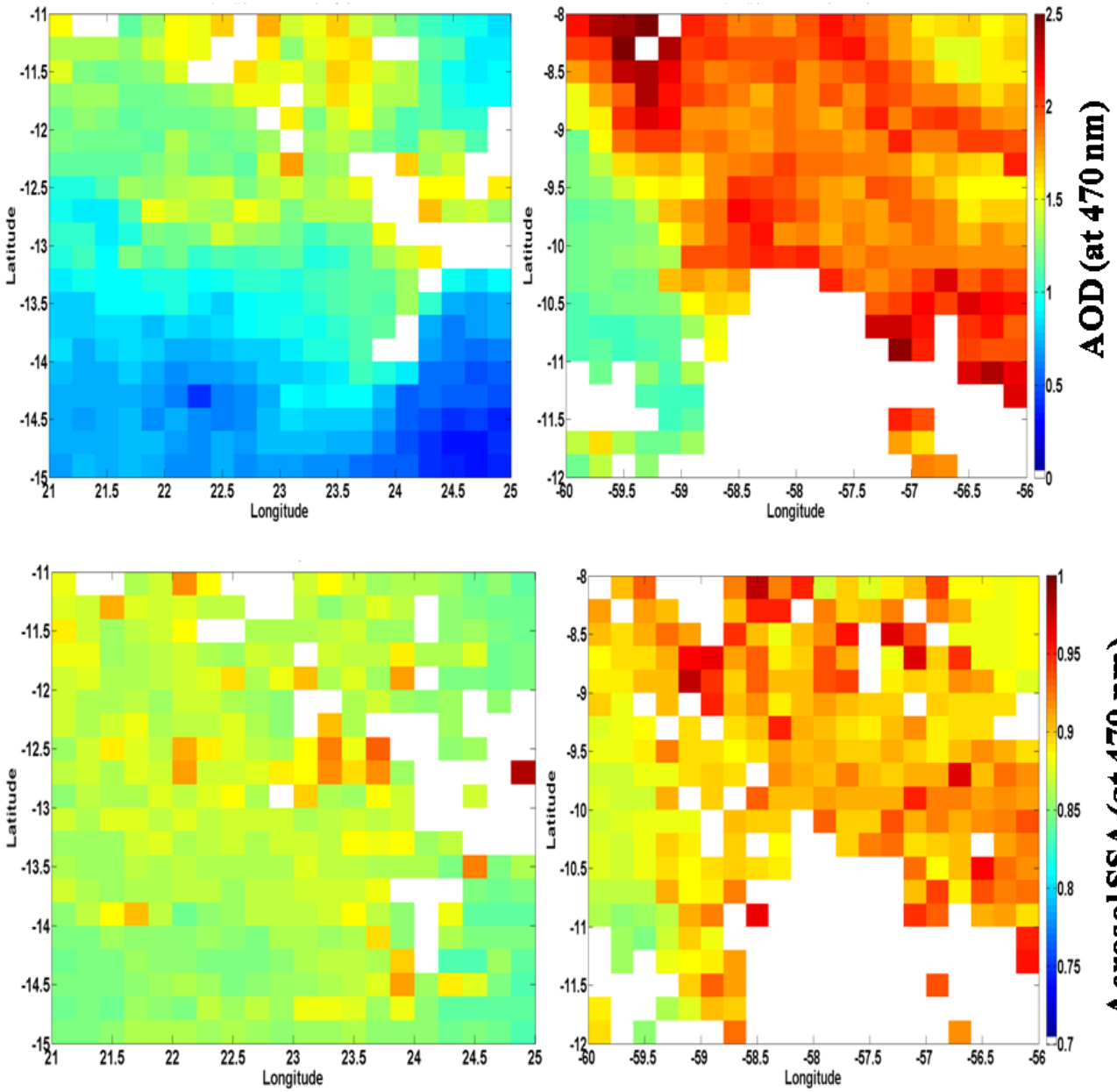

FIG. 11. Regional AOD and aerosol SSA (at 470 nm) maps. The figures on the left represent the region over South Africa with latitude = [-18 to -14] and longitude = [22 to 26] on day 250 in 2000 (day 266 as the clean day). The figures on the right represent the region over South America with latitude = [-16 to -12] and longitude = [-60 to -56] on day 252 in 2004 (with 268 as the clean day). Both images have a resolution of 20×20 km.